JVI Journals.ASM.org

Temperature-Sensitive Mutants and Revertants in the Coronavirus Nonstructural Protein 5 Protease (3CLpro) Define Residues Involved in Long-Distance Communication and Regulation of Protease Activity

Christopher C. Stobart,[b,c] Alice S. Lee,[a,c] Xiaotao Lu,[a,c] and Mark R. Denison[a,b,c]

Departments of Pediatrics[a] and Pathology, Microbiology and Immunology,[b] and The Elizabeth B. Lamb Center for Pediatric Research,[c] Vanderbilt University Medical Center, Nashville, Tennessee, USA

Positive-strand RNA virus genomes are translated into polyproteins that are processed by viral proteases to yield functional intermediate and mature proteins. Coronaviruses (CoVs) carry genes that encode an nsp5 protease (also known as 3CLpro or Mpro) responsible for 11 maturation cleavages. The nsp5 structure contains two chymotrypsin-like domains (D1 and D2) and a unique domain (D3), and forms functional dimers. However, little is known of interactions or communication across the structure of the protease during nsp5 activity. Using reverse genetic mutagenesis of the CoV murine hepatitis virus (MHV) nsp5, we identified a new temperature-sensitive (*ts*) mutation in D2 of nsp5 (Ser133Ala) and confirmed a *ts* residue in D3 (Phe219Leu). Both D2-*ts*S133A and D3-*ts*F219L were impaired for viral replication and nsp5-mediated polyprotein processing at the nonpermissive temperature. Passage of *ts*S133A and *ts*F219L at the nonpermissive temperature resulted in emergence of multiple second-site suppressor mutations, singly and in combinations. Among the second-site mutations, a D2 His134Tyr change suppressed the *ts* phenotype of D2-*ts*S133A and D3-*ts*F219L, as well as the previously reported D2-*ts*V148A. Analysis of multiple CoV nsp5 structures, and alignment of nonredundant nsp5 primary sequences, demonstrated that *ts* and suppressor residues are not conserved across CoVs and are physically distant (>10 Å) from each other, from catalytic and substrate-binding residues, and from the nsp5 dimer interface. These findings demonstrate that long-distance communication pathways between multiple residues and domains of nsp5 play a significant role in nsp5 activity and viral replication, suggesting possible novel targets for non-active site inhibitors of nsp5.

Positive-strand RNA viruses are responsible for prevalent and epidemic diseases in a wide range of vertebrate hosts, as well as new and emerging viruses, such as severe acute respiratory syndrome coronavirus (SARS-CoV), West Nile virus, and Chikungunya virus. The rapid evolution, host species movement, and diseases of positive-strand RNA viruses demonstrate the need to develop novel strategies to prevent and treat present and new diseases caused by these viruses. A key determinant of positive-strand RNA viruses is the requirement for processing of translated polyproteins by virus gene-encoded proteases. RNA virus proteases therefore have been high-profile targets for development of antiviral agents, with most protease inhibitors targeted to active sites or substrate-binding sites (21, 26, 32, 35). However, due to the potential for viral escape mutants, it is critical to identify additional noncatalytic, non-substrate-binding determinants of protease activity as potential targets for inhibition that are less prone to development of resistance.

To date, five CoVs have been shown to be associated with human respiratory diseases of different degrees of severity: human coronavirus HCoV-229E, HCoV-OC43, HCoV-NL63, HCoV-HKU1, and SARS-CoV (10, 15, 30, 31, 44, 45). CoVs contain the largest known positive-strand RNA genomes, ranging from 26 to 32 kb in length. Murine hepatitis virus (MHV) strain A59 is an established model for study of CoV replication and pathogenesis. The 32-kb genome of MHV contains seven genes, with the replicase gene (22 kb) encoding 16 nonstructural proteins (nsp1 to nsp16) (Fig. 1A) (20, 25). The replicase gene is translated into polyprotein 1a (pp1a; nsp1 to nsp11) or, via a ribosomal frameshift, pp1ab (nsp1 to nsp16) (9, 25, 33). MHV encodes two papain-like proteases (PLP1 and PLP2) responsible for cleavages of nsp1 to nsp3, and an nsp5 protease, also known as 3CLpro or Mpro, that mediates maturation cleavages of nsp4 to nsp16 and is required for virus replication (33, 50).

The CoV nsp5 is a cysteine protease present in all known CoVs and is structurally similar to the nsp4 protease of distantly related arteriviruses (6, 33, 49). The crystal structure of nsp5 has been solved for divergent CoVs from every genus, including SARS-CoV, infectious bronchitis virus (IBV), human HCoV-HKU1, and human HCoV-229E. Comparison of solved nsp5 structures demonstrates conservation of tertiary structure despite numerous differences in primary sequences (1, 2, 5, 46, 47, 49). The X-ray crystal structure of MHV nsp5 has yet to be determined; however, the structure of the closely related HCoV-HKU1 nsp5 (84% sequence identity) has been resolved to 2.5 Å (Fig. 1B and C) (49). The nsp5 proteases of all CoVs exhibit a three-domain structure, with domains 1 and 2 forming a chymotrypsin-like fold containing the His41-Cys145 catalytic dyad and substrate-binding sites (Fig. 1B) (1, 2, 5, 28, 46, 47). In contrast, domain 3 is unique to the CoV nsp5 protease among chymotrypsin-like enzymes and also shows more divergence in both sequence and structural organization between CoVs. *In vitro* studies indicate that domain 3 is important for stabilization of the chymotrypsin-like fold and may

Received 7 November 2011 **Accepted** 9 February 2012
Published ahead of print 15 February 2012
Address correspondence to Mark R. Denison, mark.denison@vanderbilt.edu.

doi:10.1128/JVI.06754-11

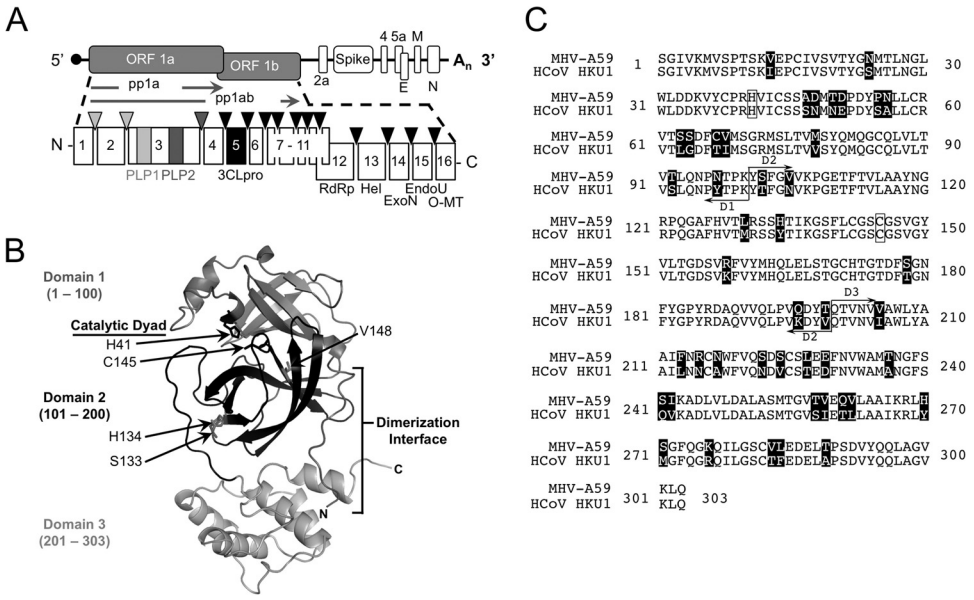

FIG 1 MHV protease nsp5 structure and sequence alignment. (A) Genome and polyprotein processing of MHV. The replicase gene (gray) consists of two open reading frames (ORF1a and ORF1ab) overlapping at a ribosomal frameshift and is translated to yield two polyprotein products, pp1a and pp1ab, encoding nonstructural proteins (nsps) nsp1 to nsp16. Maturation cleavages (arrows) are mediated by three viral proteases, papain-like proteases PLP1 (light gray) and PLP2 (dark gray) and nsp5 (black). M, matrix; E, envelope; N, nucleocapsid; RdRp, RNA-dependent RNA polymerase; Hel, helicase; ExoN, exoribonuclease; EndoU, endoribonuclease; O-MT, *O*-methyltransferase. (B) Modeled structure of a MHV nsp5 monomer based on the crystal structure of HKU1 (49) shows domain 1 (D1), domain 2 (D2), and domain 3 (D3). *ts* and second-site suppressor residues described by Sparks et al. are also identified (40). N and C denote the amino and carboxy termini. The dimerization interface is labeled, and functional residues discussed are shown in black and are labeled. (C) Sequence alignment of MHV-A59 and HCoV HKU1 with nonconserved residues highlighted, catalytic residues boxed, and domain separations identified.

also be important in mediating dimerization between nsp5 monomers (1, 28, 37, 38). Structural and biochemical studies demonstrate that nsp5 dimerization is required for proteolytic activity *in vitro* (11, 12, 37).

Recently, amino acid residues that may regulate nsp5 activity but that are distinct from the active site cavity, substrate-binding pocket, or dimerization interface have been identified. Alanine substitution at SARS-CoV nsp5 Ser147, a conserved serine residue in MHV and HKU1, disrupts dimerization and impairs nsp5 proteolytic activity, despite being greater than 9 Å from the dimerization interface (7). Our laboratory identified a temperature-sensitive (*ts*) mutation (*ts*V148A) in MHV nsp5 that impairs virus growth and nsp5 activity at 40°C (Fig. 1B) (40). Growth of the *ts*V148A mutant at 40°C resulted in emergence of second-site mutations (S133N and H134Y), which suppressed the *ts*V148A phenotype. While V148 is adjacent to the catalytic C145, neither S133N nor H134Y have predicted direct interactions with catalytic or substrate-binding residues or identified pathways for propagation of structural changes. Sawicki et al. identified a putative *ts* allele in nsp5 (F219L) at the base of unique domain 3, and distant from the dimerization interface, active site cavity, and substrate-binding regions (36). Finally, other studies have shown that nsp5 activity may be altered by changes in replicase nonstructural proteins nsp3 and nsp10 (14, 41). Together, these findings support the hypothesis that residues distant from catalytic and substrate-binding sites are important for regulating nsp5 protease activity. However, mechanisms of communication between residues and regulation of protease activity are unknown.

In this study, we tested the roles of MHV nsp5 domain 2 residues S133 and H134, and domain 3 F219, on nsp5 activity. The experiments identified a previously unknown MHV nsp5 *ts* mutation in domain 2 (*ts*S133A) and confirmed the *ts* phenotype of F219L, both of which result in profound growth and protein-processing defects at nonpermissive temperatures. Under passage at nonpermissive temperatures, a series of second-site mutations emerged that were able to suppress the *ts* phenotypes of *ts*S133A and *ts*F219L while being physically distant from the *ts* allele, the nsp5 active site cavity, and the dimerization interface. A single nonsynonymous mutation resulting in a H134Y substitution suppressed the *ts* phenotype of all three independent *ts* alleles in domains 2 and 3. The *ts* mutations reduced but did not abolish nsp5 protease activity during virus infection following a shift to the nonpermissive temperature, while individual and combined suppressor mutations restored nsp5 activity to an extent that directly correlated with increased replication. These results demonstrate the presence of multiple interconnected long-distance communication nodes in nsp5 and suggest novel mechanisms of regulation of nsp5 activity during CoV replication.

MATERIALS AND METHODS

Viruses, cells, and antisera. Recombinant wild-type (WT) MHV strain A59 (GenBank accession no. AY910861) was used as a MHV wild-type control. Delayed brain tumor cells (DBT-9), which are naturally permissive for MHV infection, and baby hamster kidney 21 cells expressing the MHV receptor (BHK-MHVR) were used for all experiments (48). Dulbecco's modified Eagle medium (DMEM) (Gibco) was supplemented with 10% heat-inactivated fetal calf serum (FCS) for all experiments described. BHK-MHVR medium was supplemented with G418 (0.8 mg/ml; CellGro) to maintain selection for MHVR expression. All biochemical experiments were carried out using rabbit polyclonal antibodies previously described in the literature. The antisera used include nsp2-specific

TABLE 1 Oligonucleotide primers used in the mutagenesis of MHV cDNA C fragment plasmids

Mutation(s) made	Primer sequence (5′ → 3′)[a]
S133A	ACG CTT CGT AGT GCC CAT ACC ATA AAG
S133A/H134Y	ACG CTT CGT AGT GCC TAT ACC ATA AAG
S133A/T129M	TTC CAT GTT ATG CTT ATG CTT CGT AGT GCC CAT ACC ATA
S133A/H134Y/T129M	TTC CAT GTT ATG CTT CGT AGT GCC TAT ACC ATA AAG
H134A	CTT CGT AGT AGC GCT ACC ATA AAG GGC
H134Y	ACG CTT CGT AGT AGC TAT ACC ATA AAG GGC TCC
F219L	AAC AGA TGC AAC TGG CTA GTG CAA AGT GAT AGT
H270HH	GCT ATT AAG AGG CTG CAT CAT TCT GGA TTC CAG
E285V	GGT AGT TGT GTG CTT GTT GAT GAG ACA CCA AGT

[a] The nucleotide changes are underlined.

(VU154), nsp5-specific (VU6), and nsp8-specific (VU123) antibodies (8, 27, 39).

Recovery of MHV mutant viruses. The MHV nsp5 mutant viruses were engineered through the infectious cDNA assembly strategy described previously by Yount et al. (48). In brief, the seven cDNA fragments were digested, gel purified, and ligated overnight at 16°C. Transcription of the extracted ligated DNA, as well as N cDNA which encodes the nucleocapsid protein, was performed by using the mMachine T7 transcription kit (Ambion) under conditions previously described in detail (48). The transcribed genome and N gene were electroporated into BHK-MHVR cells, and the electroporated cells were placed into a subconfluent flask of DBT-9 cells and incubated at either 30°C for potentially *ts* viruses or 37°C.

Mutagenesis of MHV cDNA C fragment. Assembly of the complete MHV genome is generated through the ligation of seven cDNA fragments (A to G) digested from individual plasmids as previously described by Yount et al. (48). All viruses were engineered by inserting the specified amino acid substitution into the MHV infectious clone (MHVic) C fragment containing the nsp5 sequence, which was constructed by PCR and cloned into the XL-pSMART vector (48). Sense and antisense primers were designed to be overlapping with nucleotide changes in the middle of the primer. The primers used for mutagenesis are listed in Table 1. The sequences of all mutant plasmids were confirmed prior to ligation and MHVic assembly.

RNA extraction and sequencing. A confluent monolayer of DBT-9 cells in a T25 flask was infected with viral mutant stocks at a multiplicity of infection (MOI) of 10 PFU per ml and grown until approximately 30 to 50% of the cells had formed syncytia. Supernatant was removed from each T25 flask containing isolated mutant virus and stored at −20°C. The cells were harvested in TRIzol reagent (Invitrogen) for isolation of total RNA. Reverse transcriptase PCR (RT-PCR) was performed using SuperScript III RT (Invitrogen) and random hexamers (Applied Biosystems) at 55°C for 1 h, and the resulting cDNA was PCR amplified using Easy-A high-fidelity PCR cloning enzyme (Stratagene) and MHV genome oligonucleotides covering the nsp5 region. Amplified regions were gel purified and analyzed by sequencing.

Isolation and expansion of suppressor mutants. Confluent monolayers of DBT-9 cells were initially infected with the temperature-sensitive viruses and incubated at either 40°C (S133A) or 30°C (F219L) with increases in temperature to 37°C and subsequently to 40°C. A plaque assay was then performed using 10-μl and 100-μl aliquots of viral stocks. DBT-9 cells were infected in duplicate using 6-well plates with serial dilutions of potential revertant samples with a 1-h adsorption period. The overlay contained a 1:1 mixture of 2% agar and 2× Dulbecco's modified Eagle medium. The plates were incubated for 48 h so the plaques were easily visible. Ten plaques were picked for each virus sample and resuspended in gel saline. Isolated plaques for each virus were used to infect separate T25 flasks for expansion at 40°C. The flasks were removed from nonpermissive temperatures when 70 to 95% of cells had formed syncytia, and then RNA was isolated as described above.

Analysis of viral growth and nsp5 processing. Confluent monolayers of DBT-9 cells in 60-mm dishes were infected at an MOI of 1 PFU/cell for growth analysis or 5 PFU/cell for immunoprecipitation analysis. In the temperature shift experiments, the cells were shifted from 30°C to 40°C at 6 h postinfection (p.i.). During the growth analysis, samples of supernatant were acquired and prewarmed medium was added back to maintain a fixed volume of medium for the cells. Virus titers were determined by plaque assay in duplicate. Immunoprecipitation experiments were carried out as previously described (40). Eluted proteins were resolved by sodium dodecyl sulfate-polyacrylamide gel electrophoresis (SDS-PAGE) on 4 to 12% polyacrylamide gradient Bis-Tris gels (Nu-PAGE; Invitrogen) and analyzed by autoradiography. A ^{14}C-labeled high-molecular-weight standard (New England BioLabs) and a full range rainbow marker (RPN 800E; Invitrogen) were used as protein mass standards.

Sequence alignments and modeling of MHV nsp5 structures. The X-ray crystal structure of HCoV-HKU1 nsp5 (Protein Data Bank [PDB] code 3D23) was used as a structural model of comparison (49). Structural models were generated using Modeler (16) and MacPyMol (DeLano Scientific). Other CoV nsp5 X-ray structures used for alignment and comparison were SARS (PDB code 2H2Z), HCoV-229E (PDB code 1P9T), and IBV (PDB code 2Q6D) (2, 46, 47). A query of nsp5 sequences in GenBank resulted in the identification of 432 complete coronavirus nsp5 amino acid sequences. A perl script was used to generate a representative sequence from repetitive sequences and eliminate redundancies as a means of unbiasing the data set; a final alignment of 130 unique, nonredundant sequences was prepared. A model of 100% conserved residues was determined using Consurf (4) and a sequence logo was generated using the WebLogo server (13) with the prepared nonredundant CoV nsp5 sequence data set. Distance calculations were determined by measuring from alpha carbon to alpha carbon in the structure of HCoV-HKU1 nsp5.

RESULTS

Domain 2 S133A is a novel temperature-sensitive mutant of MHV nsp5. We previously identified two second-site mutations that suppressed the temperature-sensitive phenotype of MHV *ts*V148A: H134Y and S133N (40). Both H134 and S133 are greater than 20 Å from V148, from the active site cavity, and from the S1 substrate-binding site. The mechanism by which these residues complement or suppress *ts*V148A remains unclear. Further, substitution of the H134Y or S133N residue alone in the isogenic cloned wild-type (WT) MHV background had little or no effect on virus replication at 37°C. We therefore sought to determine whether these residues had critical roles in nsp5 activity by engineering alanine substitution mutations in the MHV genome. S133A and H134A mutant viruses were recovered at 30°C and sequencing from the initial passage (passage 1 [P1]) 30°C virus stocks confirmed the presence of mutation S133A or H134A, with no other sequence changes in nsp5. The viruses were compared with recombinant WT MHV and with *ts*V148A for virus titer at 30°C and 40°C, and the efficiency of plating (EOP) was calculated (titer at 40°C/titer at 30°C) (Fig. 2A). WT MHV had an EOP of 3.3, a 3.3-fold increase in visible plaques at 40°C compared to 30°C. The previously described *ts*V148A virus exhibited an EOP of 3×10^{-5}, confirming the *ts* phenotype reported by Sparks et al. (40). The engineered H134A mutant had an EOP of 10^{-1}, which is similar to that of the previously reported engineered H134Y mutation in the WT MHV background (40). In contrast, the S133A

A

Virus Strain	Titer at:		EOP (40/30)
	30°C	40°C	
WT MHV	9×10^7	3×10^8	3×10^0
S133A	6×10^6	2×10^2	3×10^{-5}
S133A / H134Y*	2×10^7	1×10^7	5×10^{-1}
S133A / T129M / H134Y*	3×10^7	4×10^7	2×10^0
S133A / T129M^	4×10^7	5×10^4	1×10^{-3}
H134A	5×10^8	4×10^8	7×10^{-1}

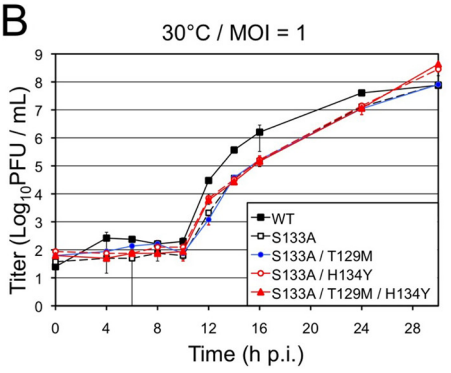

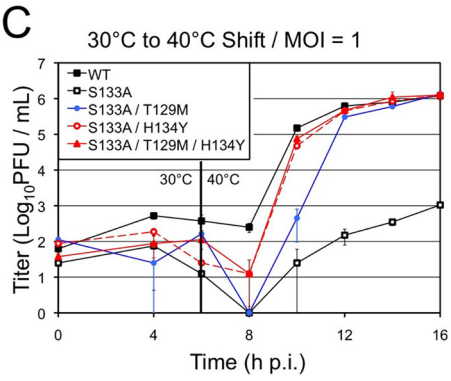

FIG 2 Analysis of replication of *ts*S133A and suppressor mutants. (A) Virus titers and EOP data for WT MHV and S133A mutant viruses determined by plaque assay at 30°C and 40°C. The virus titers were calculated in duplicate by infection of DBT-9 cells. Recombinant second-site suppressor mutants (*) and engineered recombinants whose mutations were artificially recombined (^) are indicated. (B and C) Growth analysis of the WT MHV, recombinant *ts*S133A, suppressor mutants (S133A/H134Y and S133A/T129M/H134Y), and engineered mutant (S133A/T129M) grown at 30°C (B) or grown at 30°C and then shifted to 40°C at 6 h p.i. on DBT-9 cells (C). The virus titers were determined by plaque assay on DBT-9 cells at 30°C.

mutant had an EOP of 2.7×10^{-5}, consistent with an independent *ts* phenotype (Fig. 2A). Interestingly, reversion of *ts*V148A had resulted in identification of an allele at S133 that with an Asn substitution could suppress the V148A *ts* phenotype (S133N), but with a conservative Ala substitution resulted in a new *ts* phenotype (S133A). H134A was not further examined, and *ts*S133A was studied in subsequent experiments.

Phenotypic reversion of *ts*S133A at the nonpermissive temperature reveals second-site suppressor mutations in domain 2. To test for revertants or suppressors of S133A, DBT-9 cells were infected with *ts*S133A at 37°C, followed by a shift to 40°C. Recovered supernatant virus was used to infect cells at 40°C, and 10 virus plaques were isolated and expanded at 40°C. RT-PCR sequencing of the nsp5 coding regions from all 10 clones confirmed the retention of the S133A ($_{10605}$AGC to GCC with the mutation shown underlined) engineered mutation, as well as two distinct patterns of second-site nonsynonymous mutations resulting in amino acid substitutions: H134Y ($_{10608}$CAT to $_{10608}$TAT) and T129M/H134Y ($_{10593}$ACG to $_{10593}$ATG; $_{10608}$CAT to $_{10608}$TAT). No primary reversion at S133A was identified, and no other mutations were detected in the nsp5 coding sequence. The S133A/H134Y plaque isolate had an EOP of 0.5, and the S133A/T129M/H134Y plaque isolate had an EOP of 2, suggesting almost complete suppression of the S133A *ts* phenotype (Fig. 2A). To test the contribution of the second-site mutations to suppression of the *ts* phenotype, we engineered different combinations of mutations into the isogenic cloned MHV background. Since both biologically derived suppressor mutants contained H134Y and there were subtle differences in the EOP values, we tested the independent contribution of the T129M substitution by introducing the S133A and T129M mutations in the absence of the H134Y mutation. All of the engineered recombinant mutants were readily recovered at 30°C, and sequencing confirmed that the engineered changes were present and no other mutations had arisen in nsp5. The EOPs of the recombinant S133A/H134Y and S133A/T129M/H134Y mutants were identical to the cognate biologically recovered mutant, demonstrating that the identified changes in nsp5 were necessary and sufficient for the phenotypic reversion (Fig. 2A). In contrast, the engineered recombinant S133A/T129M mutant showed an EOP of 10^{-3}, 2 log units greater than *ts*S133A but still significantly *ts* compared to either the S133A/H134Y or S133A/T129M/H134Y mutant. The results demonstrated that H134Y was sufficient for suppression of the *ts*S133A, T129M was unable to suppress the *ts* phenotype by itself, and the combination of T129M and H134Y was additive or synergistic, suggesting that they are two distinct mutations that could have arisen sequentially or concurrently in the same or different genomes.

Growth of *ts*S133A and second-site suppressor mutant viruses demonstrate differential effects of single and multiple suppressor mutations. The capacity to generate a visible plaque is one indicator of viral fitness but has limited ability to predict overall growth fitness. We therefore compared the capability of WT and mutant viruses to replicate at permissive (30°C) and nonpermissive temperatures (40°C) in single-cycle growth experiments. On the basis of earlier single-cycle growth studies of MHV replication, we infected replicate plates of DBT-9 cells with WT and recombinant mutant viruses at 30°C and a multiplicity of infection (MOI) of 1 PFU/cell (18, 19). At 6 h p.i., one replicate plate for each virus was transferred to the nonpermissive temperature of 40°C and one plate was maintained at 30°C, with supernatant samples obtained from 0 to 30 h p.i. at regular intervals for determination of viral titers. WT virus incubated at 30°C demonstrated onset of exponential growth between 10 and 12 h p.i. and achieved peak virus titers of $\sim 10^8$ PFU/cell by 30 h p.i. (Fig. 2B), consistent with previous studies (40). In contrast, *ts*S133A and all three recombinant suppressor mutant viruses demonstrated identical growth curves, with a 1-log-unit reduction in titer compared to the titer of WT MHV from 12 to 24 h p.i., but achieving titers identical to WT virus by 30 h p.i.

When the replicate virus-infected monolayers were shifted from 30°C to 40°C at 6 h p.i. (Fig. 2C), the WT virus-infected monolayers showed onset of exponential growth within 2 h after

shift and achieved peak titers between 12 and 16 h p.i., albeit at lower titers due to rapid destruction of the monolayer. The *ts*S133A mutant virus showed profoundly impaired growth for 10 h after the temperature shift. Both recombinant S133A/H134Y and S133A/T129M/H134Y mutant viruses demonstrated onset of exponential growth and peak titers similar to those of the WT virus following the shift, consistent with EOP analysis. However, the S133A/T129M virus showed a significant delay in exponential growth before achieving titers similar to those of the WT virus by 6 h after the temperature shift. These results collectively indicate that the S133A mutation confers a subtle replication defect at 30°C that is not further impaired nor complemented by the suppressor mutations and that H134Y alone or in combination with T129M is sufficient for suppression of the *ts*S133A growth phenotype. The S133A/T129M virus, while demonstrating improved growth over *ts*S133A, was still impaired compared to mutants containing H134Y, a result consistent with the EOP data, and supporting either conjecture that T129M arose first to be superseded by emergence of H134Y or arose second by conferring a subtle growth advantage of the combination over H134Y alone.

Recovery and reversion of recombinant nsp5 *ts*F219L. The experiments with *ts*S133A, in combination with our previous studies, demonstrated that the H134Y substitution was able to suppress two distinct and independently derived nsp5 *ts* alleles, *ts*V148A and *ts*S133A, suggesting an important role for intra- or intermolecular communication involved in regulation of nsp5 activity. However, both of these *ts* alleles are in domain 2 as were the suppressor mutations, and thus could not provide insight into potential long-distance communication between domains. We therefore next sought to determine whether H134 would emerge as a suppressor for another putative *ts* F219L allele in domain 3. The $_{10864}$UUU-to-CUU mutation resulting in the F219L substitution was predicted as a *ts* allele by Sawicki et al. using partial genome sequencing and reversion analysis of the *ts* mutant Alb *ts*16 (36). However, this was not confirmed in this study as the sole mutation by complete genome sequencing or by reverse genetic analysis. In addition, primary reversion occurs rapidly in biological mutants with a single-nucleotide polymorphism; therefore, possible second-site suppressors could not be identified. We engineered the F219L codon change as a two-nucleotide mutation ($_{10864}$UUU to CUA) in the isogenic MHV clone, which would require a two-nucleotide change for reversion to Phe219 (UUU or UUC). The engineered recombinant F219L mutant was recovered at 30°C, and complete genome sequencing confirmed the $_{10864}$UUU-to-CUA mutations as the only changes in the genome. The recombinant F219L mutant had an EOP of 3×10^{-5}, confirming that the F219L substitution alone was sufficient to confer a *ts* phenotype (Fig. 3A). The titer and plaque morphology of the *ts*F219L mutant were indistinguishable from those of WT MHV at 30°C (data not shown).

Identification of second-site suppressor mutations of recombinant *ts*F219L. To select for phenotypic revertants or suppressor mutations of *ts*F219L, DBT-9 cells were infected with recombinant *ts*F219L mutant virus at 40°C. However, no cytopathic effect (CPE) or productive infection occurred at 40°C, despite multiple attempts and prolonged incubation. Consequently, we initiated infection at 30°C for 6 h, followed by a shift to 37°C for 24 h. This stock was then passaged at 37°C with a shift to 40°C, followed by passage and selection of 10 plaques at 40°C. Sequencing of 10 plaque clones confirmed retention of the engineered $_{10864}$CUA (F219L) codon. However, all 10 isolated plaque cloned viruses demonstrated one of two patterns of second-site mutations in nsp5 in the presence of *ts*F219L: (i) H134Y ($_{10608}$CAT to $_{10608}$TAT)/H270 duplication (H270HH) ($_{11016}$CAT to $_{11016}$CATCAT) with an EOP of 1.2 or (ii) H134Y (CAT to TAT)/E285V ($_{11061}$GAA to $_{11061}$GTT) with an EOP of 2.9. To test the contribution of the H134Y, E285V, and H270HH changes to suppression of *ts*F219L, the identified mutations were engineered with and without F219L, alone or in the combination seen in the recovered viruses. In addition, although no F219L/

A

Virus Strain	Titer at:		EOP (40/30)
	30°C	40°C	
WT MHV	9×10^7	3×10^8	3×10^0
F219L	1×10^8	3×10^3	3×10^{-5}
F219L / H134Y / E285V*	1×10^7	4×10^7	3×10^0
F219L / H134Y / H270HH*	2×10^7	2×10^4	1×10^0
F219L / H270HH / E285V^	3×10^7	3×10^7	1×10^0
F219L / E285V^	1×10^7	2×10^2	2×10^{-5}
F219L / H134Y^	1×10^8	1×10^3	1×10^{-5}
F219L / H270HH^	8×10^6	1×10^4	2×10^{-3}

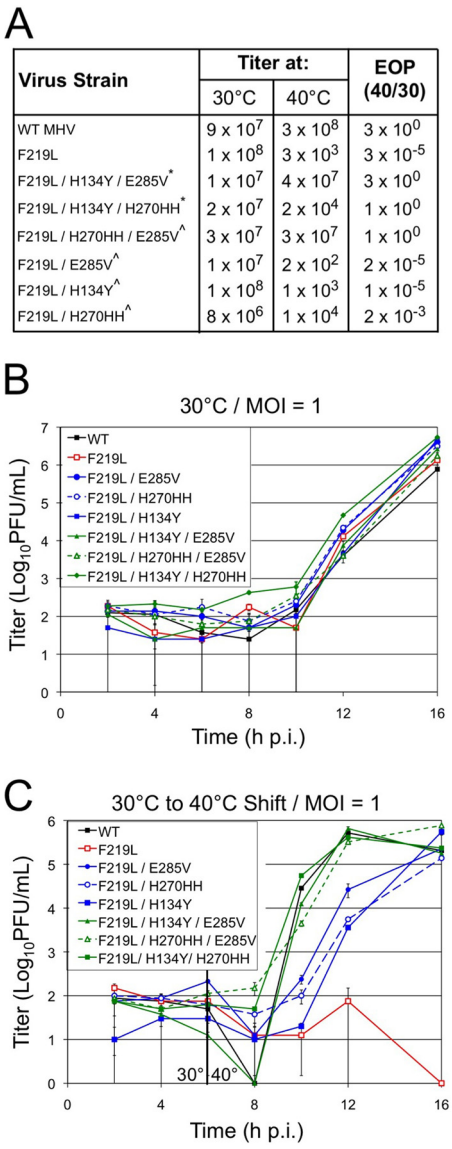

FIG 3 Analysis of replication of *ts*F219L and second-site suppressor mutants. (A) Virus titers and EOP data for WT MHV and F219L mutant viruses determined by plaque assay at 30°C and 40°C. Titers were calculated in duplicate by infection of DBT-9 cells. Recombinant second-site suppressor mutants (*) and engineered recombinants whose mutations were artificially recombined (^) are indicated. (B and C) Growth analysis of WT MHV, recombinant *ts*F219L, suppressor mutants (F219L/H134Y/E285V and F219L/H134Y/H270HH), and engineered mutants (F219L/H270HH/E285V, F219L/E285V, F219L/H270HH, and F219L/H134Y) grown at 30°C (B) or grown at 30°C and then shifted to 40°C at 6 h p.i. (C) on DBT-9 cells. The virus titers were determined by plaque assay on DBT-9 cells at 30°C.

E285V/H270HH mutant was identified among the sequenced plaques, we engineered this combination to test for the capacity of the combination to also suppress the *ts* phenotype. In total, nine genomes were engineered: F219L/E285V, F219L/H134Y, F219L/H270HH, F219L/H134Y/E285V, F219L/H134Y/H270HH, F219L/H270HH/E285V, H134Y/E285V, H134Y/H270HH, and H270HH/E285V. All viruses were recovered at 30°C with the engineered mutations detected and confirmed by sequencing across nsp5. The EOP was determined for each of the viruses by plaque assay on DBT-9 cells at 30°C and 40°C (Fig. 3A). The second-site substitution combinations identified by reversion analysis were sufficient to suppress the F219L *ts* phenotype: H134Y/E285V, EOP = 2.9; and H134Y/H270HH; EOP = 1.2. When the second-site suppressor alleles were tested alone with F219L, the results showed that the individual substitutions either minimally or partially suppressed *ts*F219L: H134Y, EOP = 2×10^{-5}; E285V, EOP = 1×10^{-5}; and H270HH, EOP = 2×10^{-3}. When the second-site substitutions were introduced in the WT background, either alone or in combination, there was no effect on EOP, suggesting that the changes were not responsible for any replication defects in the presence of F219L. The nonbiologically derived combination of F219L/E285V/H270HH also completely suppressed the *ts*F219L phenotype (F219L/E285V/H270HH, EOP = 1.0). The EOP results confirmed that the biologically identified second-site substitution combinations were both necessary and sufficient to suppress the F219L *ts* phenotype. Further, the results showed that H134Y did emerge as a suppressor allele for domain 3 *ts*F219L, but that in contrast to *ts*V148A and *ts*S133A, suppression of *ts*F219L required at least one other substitution in domain 3 in combination with H134Y.

Growth of *ts*F219L and revertants. The *ts*F219L and recombinant suppressor mutant viruses were grown in DBT-9 cells at 30°C or beginning at 30°C with a shift to 40°C at 6 h p.i. (Fig. 3B and C). At 30°C, the growth kinetics and virus yields for all mutant viruses were indistinguishable from those of WT MHV. Following the shift to 40°C at 6 h p.i., *ts*F219L showed no further replication for 10 h. In contrast, the mutant viruses containing any two of the H134Y, E285V, and H270HH substitutions showed growth after the shift to 40°C similar to WT. In contrast, all single suppressor residues expressed with F219L demonstrated a 4-h lag before exponential growth compared to the double mutants, but ultimately, they achieved peak titers similar to those of the double mutants. The titers at 10 h p.i. were consistent with the EOP data (10^{-3} to 10^{-5} compared to WT) and overall demonstrated that the individual mutations were capable of improved viral replication compared to the *ts*F219L virus yet still were *ts* compared to WT (Fig. 3A and C). Thus, in contrast to *ts*V148A and *ts*S133A, suppression of *ts*F219L appears to require a combination of at least two second-site mutations. This may be the explanation for the tight *ts*F219L phenotype at 40°C, as well as for the necessity of sequential passage of the *ts*F219 mutant virus at 30°C, 37°C, and 40°C to recover phenotypic revertants. In addition, these results identify H134Y as a second-site suppressor for a third *ts* allele in nsp5, this one in a domain 3. Overall, the results demonstrate cooperation of H134, E285, and H270 in nsp5 for efficient virus replication, as well confirming communication between nsp5 domains 2 and 3.

The *ts*S133A and *ts*F219L mutant viruses have temperature-sensitive impaired processing by nsp5. The nsp5 protease is present in all CoVs and is responsible for 11 maturation cleavage events in the replicase polyprotein (nsp4 through nsp16). To directly compare the nsp5 protease activity of *ts*V148A, *ts*S133A, *ts*F219L, and second-site suppressor mutants, DBT-9 cells were infected with WT and mutant viruses at an MOI of 5 PFU/cell and incubated at 30°C. At 6 h p.i., replicate monolayers were maintained at 30°C or transferred to 40°C, and infected cells were radiolabeled with [^{35}S]Met-Cys. Lysates from infected, radiolabeled cells were immunoprecipitated with antibodies specific for nsp2, nsp5, and nsp8 to test for processing of nsp2 by PLP1 and of nsp5 and nsp8 by nsp5.

Immunoprecipitation with antibodies specific for nsp2 of all lysates from WT and mutant virus-infected cells with labeling at 30°C and 40°C resulted in detection of mature processed nsp2, demonstrating that at both permissive and nonpermissive temperatures, there was similar translation of pp1a (nsp1 to nsp11) and normal PLP1 activity (Fig. 4). Recently, Stokes et al. reported that a *ts* mutation in nsp3 resulted in a significant decrease in nsp5-mediated processing (41). In our study, we detected the nsp4-to-nsp10 precursor polyprotein (150 kDa), which demonstrates that PLP2 is functional and is not inhibited by the nsp5 mutations (Fig. 4). The presence of mature nsp2 and the p150 bands at the nonpermissive temperature indicate that both PLP1 and PLP2 domains of nsp3 are active and are not affected by the nsp5 mutations. Although we did not test the processing of nsp3 directly, detection of both p150 and mature nsp2 is consistent with normal processing of N and C termini of nsp3. Immunoprecipitation of cells infected with WT MHV by nsp5-specific antibodies at both 30°C and 40°C resulted in detection of mature processed nsp5, as well as coimmunoprecipitation of nsp8, and two distinct small protein bands at 10 and 12 kDa, which is consistent with the predicted migration of nsp7 and nsp9. Immunoprecipitation with nsp8-specific antibodies detected nsp8 as well as probable coprecipitation of nsp5 and the 10- and 12-kDa proteins. These results show that expression and processing of pp1a proteins nsp5, nsp7, nsp8, and nsp9 are accelerated at 40°C in cells infected with WT MHV.

The temperature-sensitive viruses *ts*S133A and *ts*F219L, as well as the previously described *ts*V148A, exhibited profoundly impaired processing of nsp5 and nsp8 at 40°C compared to 30°C, indicating a specific defect in processing by the nsp5 protease. This was consistent with decreased detection of the reciprocal coimmunoprecipitating protein (nsp8 or nsp5) as well as decreased detection of the 10- and 12-kDa proteins. Although the detection of nsp5-processed proteins was profoundly decreased, we were unable from multiple replicate experiments (more than 5 experiments) to demonstrate complete loss of nsp5 activity. The results suggest that the S133A, F219L, and V148A mutations do not directly affect the catalytic or substrate-binding functions of nsp5 but rather modify protease activity in other ways. Alternatively, it is possible that the residual processing might be the result of nsp5 expressed and folded into active forms or complexes prior to the temperature shift, and thus, the protein still retains residual activity.

Viruses carrying biological and engineered suppressor mutations demonstrated restoration of processing by nsp5 that directly correlated with the degree of recovery of EOP and virus growth. Single second-site mutants S133A/T129M, F219L/H134Y, F219L/H270HH, and F219L/E285V showed an increase in detectable processed nsp5 and nsp8 only, while the double second-site suppressors restored WT-like patterns of processed proteins. Collectively, the results show a direct correlation of detection of proteins

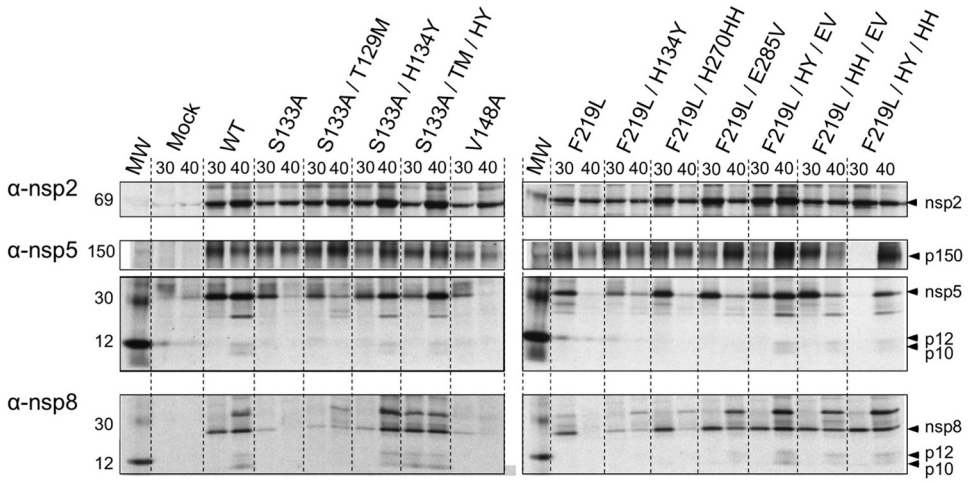

FIG 4 Proteolytic processing of WT, *ts*S133A, *ts*F219L, and suppressor viruses. DBT-9 cells were ^{35}S radiolabeled during viral infection or mock infection. Cellular lysates were harvested from cells infected with WT MHV, *ts*S133A mutants, *ts*F219L mutants, and previously described *ts*V148A and from mock-infected cells (40). Labeled proteins were immunoprecipitated using antiserum specific for nsp2, nsp5, and nsp8. The temperature during virus infection is indicated above the lanes (30°C [30] or a temperature shift from 30° to 40°C at 6 h p.i. [40]). One hundred microliters of lysate was used for all immunoprecipitations. The positions of putative viral proteins are shown to the right of the gels based upon the predicted size, and identified bands are labeled. The positions of molecular weight standards (MW) are shown to the left of the gels, and sizes are shown in kilodaltons. Protein expression profiles were resolved by SDS-PAGE and visualized by autoradiography. α-nsp2, anti-nsp2 antibody.

processed by nsp5 (nsp5 and nsp8) and the extent of restored growth fitness in culture and EOP analysis in plaque assay. Further, these findings indicate that the impairment in growth at nonpermissive temperatures is not due to complete inactivation of nsp5 protease activity.

Analysis of *ts* and suppressor mutations in nsp5 structures. To evaluate the structural relationships between the *ts* and second-site suppressor mutations, the distances between the combinations of *ts* and suppressor residues were determined by analyzing the crystal structure of the nsp5 protease of a closely related human CoV, HKU1. The structure of MHV nsp5 has not been determined; however, MHV and HKU1 nsp5 proteases exhibit 84% sequence identity (Fig. 1C) and share all of the same amino acids at the residue positions reported in this study with the exceptions of H134 and H270 (Y134 and Y270 in HKU1). All of the second-site suppressor residue positions in HKU1 nsp5 were greater than 10 Å distance from the *ts* residues in the monomeric structure with the sole exception that the H134 residue is 3.8 Å from the juxtaposed S133 (data not shown). Measurement of the distance between residues in different monomers of the dimeric structure of both SARS-CoV and HKU1 nsp5 demonstrated that no two residues from this study were closer than 15.0 Å. Measurement of the distance between the *ts* and second-site suppressor mutants and the catalytic dyad residues, H41 and C145, showed that only V148A was within 10 Å of either residue. Collectively, these data demonstrate that the relationship between the *ts* and suppressor mutations cannot be explained by direct interactions between residues and that nsp5 dimerization does not provide direct intermonomer associations between the residues identified in this study. Modeling of the S133A and F219L mutations on the structure of HKU1 nsp5 failed to predict any clear pathways of side chain remodeling or perturbation between the *ts* residues and the protease active site (data not shown). In contrast, analysis of residue conservation using an alignment of 130 nonredundant CoV nsp5 amino acid sequences identified a series of 100% identical residues that span the regions of nsp5 between each of the *ts* residues (S133, V148, and F219) and the common second-site suppressor residue (H134) (Fig. 5). These findings indicate that the structural and functional perturbations on nsp5 protease of the *ts* mutations may span long distances across the protease structure through yet to be identified cooperative interactions.

Residue conservation of *ts* and suppressor alleles is group specific. To evaluate the variability at the *ts* and suppressor alleles,

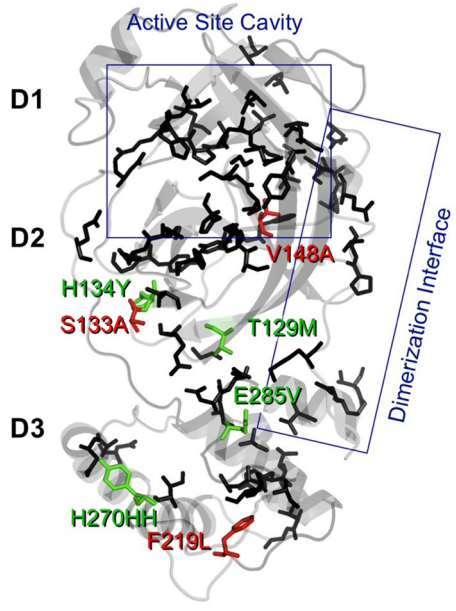

FIG 5 Conserved, *ts*, and suppressor alleles in a solved CoV nsp5 structure. A conservation map of 100% identical nsp5 residues (black) across 130 nonredundant CoV nsp5 sequences is shown on the HKU1 nsp5 protease monomer structure. The locations of identified *ts* alleles (red) and suppressor alleles (green) are indicated.

A

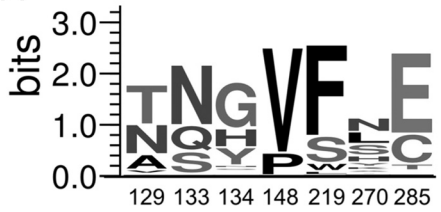

B

MHV Residue Position:	129	133	134	148	219	270	285
Genus: Alphacoronavirus							
α-CoV1 (TGEV)	N	Q	G	V	F	N	C
HCoV 229E	N	N	W	P	W	N	N
HCoV NL63	N	N	F	P	W	H	C
PEDV	N	N	Y	P	W	H	T
BtCoV HKU2	N	T	H	P	W	A	T
BtCoV 512/05	N	N	Y	P	W	H	C
BtCoV 1A	I	N	K	P	F	A	T
BtCoV HKU8	T	N	Y	P	F	A	T
Genus: Betacoronavirus							
MHV-A59	T	S	H	V	F	H	E
β-CoV1 (HCoV OC43)	T	S	Y	V	F	K	E
HCoV HKU1	T	S	Y	V	F	Y	E
BtCoV HKU9	T	N	G	P	F	L	E
BtCoV HKU4	N	N	S	V	F	H	E
BtCoV HKU5	N	Q	H	V	F	H	E
SARS-CoV Urbani	A	N	H	V	F	Q	E
Genus: Gammacoronavirus							
Avian Coronavirus (IBV)	T	N	G	V	S	S	E
Beluga Whale CoV SW1	T	N	G	V	F	A	E

FIG 6 Coronavirus protein sequence conservation of *ts* and suppressor alleles. (A) A sequence logo of conservation of *ts* and suppressor mutations across an alignment of 130 nonredundant CoV nsp5 sequences was generated using WebLogo (13). The height of each letter corresponds to the relative conservation of that amino acid at the position, and the height of the column corresponds to the sequence conservation at the position. The residue numbers are relative to the MHV amino acid positions. (B) The *ts* and suppressor residues of coronavirus species by CoV genus are shown for each MHV residue position. α-CoV1, alphacoronavirus 1; TGEV, transmissible gastroenteritis virus; PEDV, porcine epidemic diarrhea virus; BtCoV, bat coronavirus.

a sequence logo (13) was generated using the nonredundant alignment of 130 CoV nsp5 amino acid sequences, and the *ts* and suppressor alleles for 17 coronavirus species were analyzed (Fig. 6A and B). From two to eight different residues occupy each position across available CoV sequences (Fig. 6A). Surprisingly, the H134Y common second-site suppressor mutation selected for a tyrosine that is already present in several betacoronaviruses. Further, the S133N second-site suppressor first reported by Sparks et al. is common as an Asn in many coronaviruses (40). Conservation of distinct *ts* and suppressor alleles within the three genera suggest that there may be select combinations of alleles that are necessary for nsp5 activity (Fig. 6B). These findings further suggest that alterations in structure attributed to these residues could have analogous combinations in other CoVs.

DISCUSSION

Previous studies with other viruses as diverse as HIV, Sindbis virus, poliovirus, and vaccinia virus have reported *ts* mutations in virus proteases that affect protein processing, RNA synthesis, and virus capsid assembly (3, 23, 24, 29). Most of the *ts* alleles of described viral proteases have occurred at individual conserved residues or in pairs of conserved and structurally adjacent residues. For the HIV protease, residues distant from known catalytic and functional determinants have been shown to be critical for protease activity (22, 34). The current study of MHV nsp5 (3CLpro) extends our understanding of RNA virus proteases by demonstrating that multiple nonconserved and structurally distant residues in the CoV nsp5 protease participate in long-distance communication within and between the protease structural domains, function cooperatively to suppress *ts* phenotypes, and are important for nsp5 activity during replicase polyprotein processing. Specifically, we demonstrate that independent and physically distant *ts* alleles in domains 2 and 3 resulted in selection of the same H134Y *ts* suppressor allele, as well as selection of several additional suppressor alleles. With the exception of *ts*V148A, all of the residues are structurally distant from the catalytic, substrate, and dimerization residues in monomers and between nsp5 molecules in solved nsp5 dimer structures. In addition, suppressor mutations arose during reversion analysis in combinations that were required for or augmented restoration of nsp5 processing. Further, artificial combinations of suppressor mutations not seen during biological reversion analysis also showed cooperative suppression of the *ts* phenotype. These results all support the hypothesis that long-distance communication occurs between multiple residue nodes to regulate nsp5 activity.

Since nsp5 must recognize and process 11 closely related cleavage sites in the setting of rapidly changing substrate and cleavage site concentrations from polyproteins and processing intermediates, any explanation for nsp5 intra- or intermolecular communication needs to account for these evolving variables. The observation that a series of residues that are completely conserved across the coronaviruses span the regions between the *ts* and second-site mutations in solved and modeled CoV nsp5 structures (Fig. 5) suggests a possible mechanism for such communication. The potential linkage by conserved residues in the nsp5 tertiary structure would be similar to the model proposed by Ranganathan and coworkers in which networks of distant residues are connected in tertiary structure and are nodes for allosteric communication (22, 42). These networks may further demonstrate coevolution of residues that maintain the protease structure.

Temperature-sensitive mutations and nsp5 activity. Analyses of the MHV nsp5 *ts* mutant viruses demonstrated a defect in nsp5-mediated processing and virus replication at the nonpermissive temperature. However, mature nsp5 cleavage products were still detected for all three *ts* mutant viruses at the nonpermissive temperature, albeit at profoundly reduced levels, indicating that defects in viral growth at the nonpermissive temperature were not the result of complete loss of nsp5 activity. We previously reported that nsp5 activity was not present in *ts*V148A at the nonpermissive temperature, but in that study we did not test nsp5 processing at cleavage sites flanking nsp5. In the present study, we determined that *ts*V148A functions like *ts*S133A and *ts*F219L, exhibiting more impaired processing of nsp8 than nsp5 at the nonpermissive temperature, while retaining residual nsp5 activity at the flanking nsp4-nsp5 and nsp5-nsp6 cleavage sites (40). Overall, our results suggest that the nsp5 *ts* phenotype may be due to an alteration of protease activity at different polyprotein substrate sites. Altered cleavage site specificity has been reported for mutations introduced in the interdomain loop between domains 2 and 3 of the arterivirus equine arteritis virus (EAV) nsp4 protease, a structural orthologue of CoV nsp5 (43). Several of the recovered EAV nsp4 interdomain loop mutants did not abolish nsp4 protease activity but rather altered the substrate specificity. It is possible that the *ts* mutants of nsp5 are acting in a similar manner.

Nonconserved residues in nsp5 protease function. Align-

ment of 130 nonredundant CoV nsp5 sequences demonstrates that the residues that resulted in the nsp5 *ts* mutations are not conserved. There was more conservation of specific residues within the betacoronavirus genus, including MHV and SARS-CoV, specifically at residues V148, F219L, and E285. Finally, the revertants H134Y and S133N selected amino acids that already were present in nsp5 sequences of other alpha- and betacoronaviruses. Among the second-site residues, the H270 position shows the greatest variation with eight different amino acid residues tolerated across the CoVs. The tolerance for a wide variety of residues at this position may explain the acceptance of a duplicated codon resulting in a second histidine residue at the position. While the results have to be interpreted in light of the overall nsp5 sequence variability or conservation, they suggest that the *ts* and revertant residues may represent an evolutionarily adaptive network co-evolving with other interacting proteins or cleavage sites. In support of this hypothesis, it was reported that a mutation at the P1 position in the cleavage site between nsp15 and nsp16 of the CoV infectious bronchitis virus resulted in a debilitated virus whose phenotype was compensated for by a mutation in nsp5 (17). Similarly, *ts* mutations in MHV nsp3 and nsp10 resulted in altered nsp5-mediated nsp5 processing (14, 41). A network of nonconserved and mutationally flexible residues could account for the rapid emergence of second-site revertants of *ts* viruses with combinations of more than one second-site mutation that also function in combinations not derived during virus reversion analysis.

Models for testing nsp5 long-distance communication. Coronavirus nsp5 functions in the setting of the largest known RNA virus polyprotein and must orchestrate 11 distinct cleavage events. It is clear from our findings and others that nsp5 activity is affected by changes within the structure of the protease, by changes at nsp5 cleavage sites, and by changes in other replicase proteins. Biochemical studies of the *ts* and revertant nsp5 molecules from this study should determine whether protein alterations and communication are intramolecular or within the nsp5 dimer. Continued mutagenesis of nsp5 in the context of a virus will permit testing for allosteric interactions across the replicase polyprotein that impact specific *ts* and revertant alleles during virus replication. To test for additional communication nodes in nsp5, we will continue to use an iterative approach for mutagenesis at *ts* and revertant alleles with alanine, nonconservative changes, and substitution of residues from other CoV nsp5 sequences. Finally, since some of the MHV revertant alleles such as H134Y are already present in other CoVs, it may be possible to test whether the variability at the revertant residues across different coronaviruses affects whether a particular substitution results in a *ts* phenotype in different nsp5 backgrounds. The application of this data set in combination with structure information and bioinformatic analysis should allow dissection of the extent and mechanism of the communication network that regulates nsp5 activity during coronavirus replication.

ACKNOWLEDGMENTS

We thank Dia Beachboard, Michelle Becker, Megan Culler, Lance Eckerle, Mark Gadlage, and Wayne Hsieh for technical assistance and helpful advice regarding manuscript preparation. We also thank Andrew Mesecar, Aimee Eggler, and Sakshi Tomar for helpful conversations and suggestions in preparing the manuscript and Eric Donaldson for assistance in preparing and using the multiple-sequence alignment for the manuscript.

Support for this work was provided by National Institutes of Health grant R01AI26603 (M.R.D.) from the National Institute of Allergy and Infectious Disease and the Virology Training Grant T32 AI089554 (C.C.S.) through Vanderbilt University. This work was also supported by The Elizabeth B. Lamb Center for Pediatric Research.

REFERENCES

1. **Anand K, et al.** 2002. Structure of coronavirus main proteinase reveals combination of a chymotrypsin fold with an extra alpha-helical domain. EMBO J. **21**:3213–3224.
2. **Anand K, Ziebuhr J, Wadhwani P, Mesters JR, Hilgenfeld R.** 2003. Coronavirus main proteinase (3CLpro) structure: basis for design of anti-SARS drugs. Science **300**:1763–1767.
3. **Ansarah-Sobrinho C, Moss B.** 2004. Role of the I7 protein in proteolytic processing of vaccinia virus membrane and core components. J. Virol. **78**:6335–6343.
4. **Ashkenazy H, Erez E, Martz E, Pupko T, Ben-Tal N.** 2010. ConSurf 2010: calculating evolutionary conservation in sequence and structure of proteins and nucleic acids. Nucleic Acids Res. **38**:W529–W533.
5. **Bacha U, et al.** 2008. Development of broad-spectrum halomethyl ketone inhibitors against coronavirus main protease 3CL(pro). Chem. Biol. Drug Des. **72**:34–49.
6. **Barrette-Ng IH, et al.** 2002. Structure of arterivirus nsp4.The smallest chymotrypsin-like proteinase with an alpha/beta C-terminal extension and alternate conformations of the oxyanion hole. J. Biol. Chem. **277**: 39960–39966.
7. **Barrila J, Bacha U, Freire E.** 2006. Long-range cooperative interactions modulate dimerization in SARS 3CLpro. Biochemistry **45**:14908–14916.
8. **Bost AG, Carnahan RH, Lu XT, Denison MR.** 2000. Four proteins processed from the replicase gene polyprotein of mouse hepatitis virus colocalize in the cell periphery and adjacent to sites of virion assembly. J. Virol. **74**:3379–3387.
9. **Brierley I, Digard P, Inglis SC.** 1989. Characterization of an efficient coronavirus ribosomal frameshifting signal: requirement for an RNA pseudoknot. Cell **57**:537–547.
10. **Cavallaro JJ, Monto AS.** 1970. Community-wide outbreak of infection with a 229E-like coronavirus in Tecumseh, Michigan. J. Infect. Dis. **122**: 272–279.
11. **Chen H, et al.** 2006. Only one protomer is active in the dimer of SARS 3C-like proteinase. J. Biol. Chem. **281**:13894–13898.
12. **Chen S, et al.** 2008. Mutation of Gly-11 on the dimer interface results in the complete crystallographic dimer dissociation of severe acute respiratory syndrome coronavirus 3C-like protease: crystal structure with molecular dynamics simulations. J. Biol. Chem. **283**:554–564.
13. **Crooks GE, Hon G, Chandonia JM, Brenner SE.** 2004. WebLogo: a sequence logo generator. Genome Res. **14**:1188–1190.
14. **Donaldson EF, Graham RL, Sims AC, Denison MR, Baric RS.** 2007. Analysis of murine hepatitis virus strain A59 temperature-sensitive mutant TS-LA6 suggests that nsp10 plays a critical role in polyprotein processing. J. Virol. **81**:7086–7098.
15. **Drosten C, et al.** 2003. Identification of a novel coronavirus in patients with severe acute respiratory syndrome. N. Engl. J. Med. **348**:1967–1976.
16. **Eswar N, Eramian D, Webb B, Shen MY, Sali A.** 2008. Protein structure modeling with MODELLER. Methods Mol. Biol. **426**:145–159.
17. **Fang S, Shen H, Wang J, Tay FP, Liu DX.** 2010. Functional and genetic studies of the substrate specificity of coronavirus infectious bronchitis virus 3C-like proteinase. J. Virol. **84**:7325–7336.
18. **Gadlage MJ, Denison MR.** 2010. Exchange of the coronavirus replicase polyprotein cleavage sites alters protease specificity and processing. J. Virol. **84**:6894–6898.
19. **Gadlage MJ, et al.** 2010. Murine hepatitis virus nonstructural protein 4 regulates virus-induced membrane modifications and replication complex function. J. Virol. **84**:280–290.
20. **Gorbalenya AE, Koonin EV, Donchenko AP, Blinov VM.** 1989. Coronavirus genome: prediction of putative functional domains in the nonstructural polyprotein by comparative amino acid sequence analysis. Nucleic Acids Res. **17**:4847–4861.
21. **Grum-Tokars V, Ratia K, Begaye A, Baker SC, Mesecar AD.** 2008. Evaluating the 3C-like protease activity of SARS-coronavirus: recommendations for standardized assays for drug discovery. Virus Res. **133**:63–73.
22. **Halabi N, Rivoire O, Leibler S, Ranganathan R.** 2009. Protein sectors: evolutionary units of three-dimensional structure. Cell **138**:774–786.
23. **Kaplan AH, Manchester M, Smith T, Yang YL, Swanstrom R.** 1996.

Conditional human immunodeficiency virus type 1 protease mutants show no role for the viral protease early in virus replication. J. Virol. **70**:5840–5844.
24. **Kean KM, Agut H, Fichot O, Wimmer E, Girard M.** 1988. A poliovirus mutant defective for self-cleavage at the COOH-terminus of the 3C protease exhibits secondary processing defects. Virology **163**:330–340.
25. **Lee HJ, et al.** 1991. The complete sequence (22 kilobases) of murine coronavirus gene 1 encoding the putative proteases and RNA polymerase. Virology **180**:567–582.
26. **Lu G, et al.** 2011. Enterovirus 71 and coxsackievirus A16 3C proteases: binding to rupintrivir and their substrates and anti-hand, foot, and mouth disease virus drug design. J. Virol. **85**:10319–10331.
27. **Lu X, Lu Y, Denison MR.** 1996. Intracellular and in vitro-translated 27-kDa proteins contain the 3C-like proteinase activity of the coronavirus MHV-A59. Virology **222**:375–382.
28. **Lu Y, Denison MR.** 1997. Determinants of mouse hepatitis virus 3C-like proteinase activity. Virology **230**:335–342.
29. **Mayuri Geders TW, Smith JL, Kuhn RJ.** 2008. Role for conserved residues of Sindbis virus nonstructural protein 2 methyltransferase-like domain in regulation of minus-strand synthesis and development of cytopathic infection. J. Virol. **82**:7284–7297.
30. **McIntosh K, Becker WB, Chanock RM.** 1967. Growth in suckling-mouse brain of "IBV-like" viruses from patients with upper respiratory tract disease. Proc. Natl. Acad. Sci. U. S. A. **58**:2268–2273.
31. **McIntosh K, Dees JH, Becker WB, Kapikian AZ, Chanock RM.** 1967. Recovery in tracheal organ cultures of novel viruses from patients with respiratory disease. Proc. Natl. Acad. Sci. U. S. A. **57**:933–940.
32. **Nguyen TT, et al.** 2011. Virtual screening identification of novel severe acute respiratory syndrome 3C-like protease inhibitors and in vitro confirmation. Bioorg. Med. Chem. Lett. **21**:3088–3091.
33. **Perlman S, Netland J.** 2009. Coronaviruses post-SARS: update on replication and pathogenesis. Nat. Rev. Microbiol. **7**:439–450.
34. **Perryman AL, Lin JH, McCammon JA.** 2004. HIV-1 protease molecular dynamics of a wild-type and of the V82F/I84V mutant: possible contributions to drug resistance and a potential new target site for drugs. Protein Sci. **13**:1108–1123.
35. **Poordad F, Khungar V.** 2011. Emerging therapeutic options in hepatitis C virus infection. Am. J. Manag. Care. **17**:S123–S130.
36. **Sawicki SG, et al.** 2005. Functional and genetic analysis of coronavirus replicase-transcriptase proteins. PLoS Pathog. **1**:e39.
37. **Shi J, Sivaraman J, Song J.** 2008. Mechanism for controlling the dimer-monomer switch and coupling dimerization to catalysis of the severe acute respiratory syndrome coronavirus 3C-like protease. J. Virol. **82**:4620–4629.
38. **Shi J, Song J.** 2006. The catalysis of the SARS 3C-like protease is under extensive regulation by its extra domain. FEBS J. **273**:1035–1045.
39. **Sims AC, Ostermann J, Denison MR.** 2000. Mouse hepatitis virus replicase proteins associate with two distinct populations of intracellular membranes. J. Virol. **74**:5647–5654.
40. **Sparks JS, Donaldson EF, Lu X, Baric RS, Denison MR.** 2008. A novel mutation in murine hepatitis virus nsp5, the viral 3C-like proteinase, causes temperature-sensitive defects in viral growth and protein processing. J. Virol. **82**:5999–6008.
41. **Stokes HL, et al.** 2010. A new cistron in the murine hepatitis virus replicase gene. J. Virol. **84**:10148–10158.
42. **Suel GM, Lockless SW, Wall MA, Ranganathan R.** 2003. Evolutionarily conserved networks of residues mediate allosteric communication in proteins. Nat. Struct. Biol. **10**:59–69.
43. **van Aken D, Snijder EJ, Gorbalenya AE.** 2006. Mutagenesis analysis of the nsp4 main proteinase reveals determinants of arterivirus replicase polyprotein autoprocessing. J. Virol. **80**:3428–3437.
44. **van der Hoek L, et al.** 2004. Identification of a new human coronavirus. Nat. Med. **10**:368–373.
45. **Woo PC, et al.** 2005. Characterization and complete genome sequence of a novel coronavirus, coronavirus HKU1, from patients with pneumonia. J. Virol. **79**:884–895.
46. **Xue X, et al.** 2007. Production of authentic SARS-CoV M(pro) with enhanced activity: application as a novel tag-cleavage endopeptidase for protein overproduction. J. Mol. Biol. **366**:965–975.
47. **Xue X, et al.** 2008. Structures of two coronavirus main proteases: implications for substrate binding and antiviral drug design. J. Virol. **82**:2515–2527.
48. **Yount B, Denison MR, Weiss SR, Baric RS.** 2002. Systematic assembly of a full-length infectious cDNA of mouse hepatitis virus strain A59. J. Virol. **76**:11065–11078.
49. **Zhao Q, et al.** 2008. Structure of the main protease from a global infectious human coronavirus, HCoV-HKU1. J. Virol. **82**:8647–8655.
50. **Ziebuhr J, Snijder EJ, Gorbalenya AE.** 2000. Virus-encoded proteinases and proteolytic processing in the Nidovirales. J. Gen. Virol. **81**:853–879.